7

Reinforcement Effects of CNTs for Polymer-Based Nanocomposites

Yuan Li, Yaolu Liu and Ning Hu
Chiba University
Japan

1. Introduction

With large aspect ratio, high strength and stiffness, carbon nanotubes (CNTs) have been widely used as the reinforcement for polymer-based nanocomposites with prospective application in aerospace engineering, automotive industry, etc. Generally, there are two typical representatives: three-phase hybrid CFRP laminates (CNT/Polymer/CF) and two-phase CNT-reinforced polymer (CNT/Polymer) nanocomposites.

For **three-phase hybrid CFRP laminates** which use CNTs to improve the interlaminar mechanical properties of CFRP laminates, the fabrication methods can be categorized into the following three ways:

i. *Matrix reinforcement*, which uses the two-phase CNT/Polymer nanocomposites as the matrix for CFRP plies before lay-up [Yokozeki et al., 2007; Karapappas et al., 2009; Inam et al., 2010];
ii. *Filler reinforcement*, which employs the CNT-grafted carbon fibres as reinforcement filler for CFRP plies before lay-up [Thostenson et al., 2002; Veedu et al., 2006; He et al., 2007; Kepple et al., 2008];
iii. *Interface reinforcement*, which adds CNTs into the interface between CFRP plies during lay-up [Garcia et al., 2008; Arai et al., 2008].

Although great progress has been made for the first two ways, less work is reported on the third one.

Therefore, in the present work, a newly simple fabrication method, i.e., **Powder method** *was developed to disperse the CNTs at the interface between CFRP plies. The improvement of interlaminar mechanical properties was investigated by DCB (double cantilever bending) tests and FEM (finite element method) analysis.*

For **two-phase CNT/Polymer nanocomposites**, numerous experimental investigations have been carried out on the reinforcement effect of CNTs addition in thermosetting ones, e.g. epoxy [Schadler et al., 1998; Gojny et al., 2005; Ci & Bai, 2006], polyimide [Ogasawara et al., 2004; Jiang et al., 2005], and phenolic [Tai et al., 2004], as well as thermoplastic ones, e.g. polypropylene (PP) [Bhattacharyya et al., 2003; Chang et al., 2005], polystyrene (PS) [Thostenson & Chou, 2002; Chang et al., 2006], polymethylmethacrylate (PMMA) [Cooper et al., 2002; Lee et al., 2006] and polyether ether kentone (PEEK) [Deng et al., 2007; Bangarusampath et al., 2009]. However, the reported improvement of mechanical properties of these nanocomposites is far more less than the expectation because of poor dispersion, difficult alignment of CNTs, and weak interface between CNT and polymer matrix, which

are involved in geometrical properties of CNTs themselves, polymer properties, fabrication method of CNT/Polymer nanocomposites.

To overcome these obstacles, various efforts, such as ultrasonication [Safadi et al., 2002; Ding et al., 2003], surface treatment [Curran et al. 1999; Vigolo et al., 2000; Gojny et al., 2003], shear mixing [Andrews et al., 2002], bi/tri-axial rolling [Rosca & Hoa, 2009; Gojny et al., 2004], extrusion [Cooper et al., 2002; Wong et al., 2003], and their combination, have been firstly made to effectively achieve good dispersion of CNTs in polymer. Moreover, several techniques have been proposed to control CNTs alignment using shear [Ajayan et al., 1994], elongation [Jin et al., 1998], melt processing [Haggenmueller et al., 2000], as well as magnetic field [Kimura et al., 2003] or electrical spinning [Sen et al., 2004]. Furthermore, great progress has been made on the investigation of the interfacial properties. For example, direct CNT pull-out experiments were made in telescope electron microscopy (TEM) [Qian et al., 2000; Deng, 2008], or by atomic force microscopy (AFM) [Barber et al., 2003, 2004], Raman spectroscopy [Schadler et al., 1998], scanning probe microscope (SPM) [Cooper et al., 2002]. However, difficult manipulation in nano-scale and measurement on force/displacement makes large data scattering inevitable, which makes numerical simulation a powerful alternative approach. Continuum mechanical, molecular mechanics (MM), conventional or ab initio molecular dynamics (MD), or their combinations, have also been attempted to investigate the interfacial properties. For instance, some continuum mechanics based models (e.g. cohesive zone model [Jiang et al., 2006], shear lag model [Xiao & Zhang, 2004; Gao & Li, 2005; Tsai & Lu, 2009], and pull-out model [Lau, 2003; Natsuki et al., 2007]) were developed to investigate the interfacial properties between CNT and polymer matrix. Compared with Natsuki's suggestion [Natsuki et al., 2007] of that maximum interfacial shear stress (ISS) occurs at the pull-out end of CNT, Gao [Gao & Li, 2005] predicted that ISS approaches maximum at the two ends of CNT, but keeps zero at the middle part. On the other hand, most of MM/MD simulations [Lordi & Yao, 2000; Liao & Li, 2001; Frankland et al., 2002; Gou et al., 2004; Zheng et al., 2009; Al-Ostaz et al., 2008; Chowdhury & Okabe, 2007] assumed constant ISS during the whole pull-out process with uniform distribution along the contact surface between CNT and polymer. Obviously, the above totally different distribution forms of ISS leads to great confusion in understanding the inherent interfacial characteristics of CNT/Polymer nanocomposites. Moreover, all of the previous MM/MD simulations are limited to a specified SWCNT with a fixed length and diameter. The influences of CNTs' dimension on the pull-out behaviour have never been investigated.

Therefore, in the present work, the other focus is put on the clarification of interfacial properties between CNT and polymer matrix, in which the effects of CNTs' dimension (i.e. nanotube length, diameter and wall number) were explored for the first time. Moreover, the obtained interfacial properties were combined with the theoretical model of continuum mechanics to develop a sequential multi-scale model for predicting the overall mechanical properties of CNT/Polymer nanocomposites, which were verified using tensile tests and SENB (single-edge notched bending) tests.

Here, two commercial CNTs products, i.e. MWCNT-7 (Nano Carbon Technologies Co., Ltd. Japan) and VGCF® (Showa Denko K.K., Japan) as shown in Fig. 1, were employed as reinforcement fillers at the interface of conventional CFRP laminates to fabricate three-phase hybrid CFRP laminates, and in epoxy to fabricate two-phase CNT/Polymer nanocomposites, respectively. The average diameter of VGCF® is around two times higher than that of MWCNT-7. Moreover, wall thickness of VGCF® is larger, while the central wall is much smaller than that of MWCNT-7. The corresponding geometrical and mechanical properties of these two CNTs are listed in Table 1.

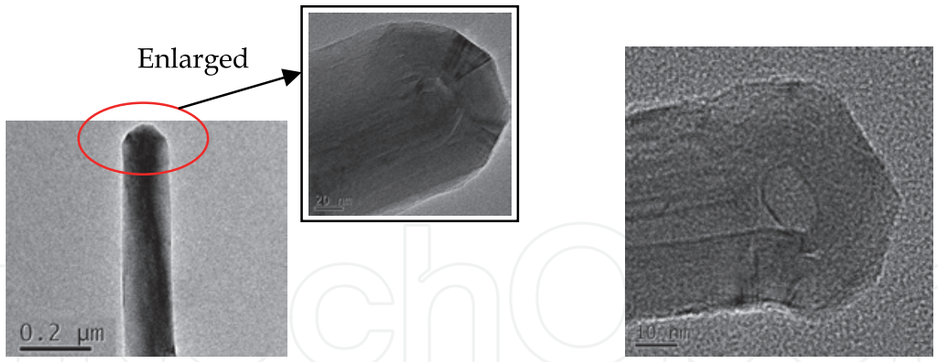

(a) VGCF® (b) MWCNT-7

Fig. 1. TEM pictures of two commercial CNTs

CFRP prepregs		Commercial CNTs	VGCF®	MWCNT-7
Matrix	#2500	Radius r_f (nm)	75	32.5
PAN-based CF	T700S	Length l_f (μm)	15 (10~20)	7.5 (5~10)
Young's modulus (GPa)		Density ρ_f (kg/m^3)	2.0	2.1
Fibre direction	116.8	Young's modulus E_f (GPa)	516.5 (273~760)	850 [Demczyk et al., 2002]
Transverse direction	8.83	Tensile strength σ_{ultf} (MPa)	3100 (2700~3500)	1.5×10^5 [Demczyk et al., 2002]

Table 1. Properties of CFRP prepregs and two commercial CNTs

2. Three-phase hybrid CFRP laminates

Powder method was developed to disperse CNTs directly at the interface between CFRP prepregs to fabricate three-phase hybrid CFRP laminates. The improvement on the interlaminar mechanical properties was confirmed by DCB tests and FEM analysis.

2.1 DCB experiments

2.1.1 Materials and specimen fabrication

The CFRP prepregs (T700S/#2500 Toray, Co. Ltd., Japan) were used, where their physical and mechanical properties are also given in Table 1.

Here, CNTs, as the reinforcement at interface, was dispersed at the mid-plane of unidirectional $[0^\circ/0^\circ]_{14}$ CFRP laminates during the hand lay-up process, where a simple fabrication method with low cost, i.e. **powder method**, was employed. The detailed process is described in Fig. 2 as below.

a. Initially, 14 pieces of CFRP plies were stacked together to form two pieces of $[0^\circ]_7$ CFRP unidirectional sublaminates, respectively;
b. CNTs powder was spread by half on the surface of lower sublaminate using a sifter with mesh size about 70μm. The zigzagged spreading path makes the distribution of CNTs at the interface as consistent as possible;
c. The left half of CNTs powder was spread after placing a 25 μm thick polyamide film (Kapton, Toray Co. Ltd., Japan) to make an initial crack;

d. The upper sublaminate was piled up;
e. Finally, it was put into an autoclave for 3 hours at the temperature of 130°C to cure.

The obtained laminates are typed in Table 2 according to CNTs' area density ρ_A at the interface. Obviously, the measured thicknesses of formed CNTs interlayer t_I increases linearly with area density ρ_A. For reference, base CFRP laminates were also fabricated.

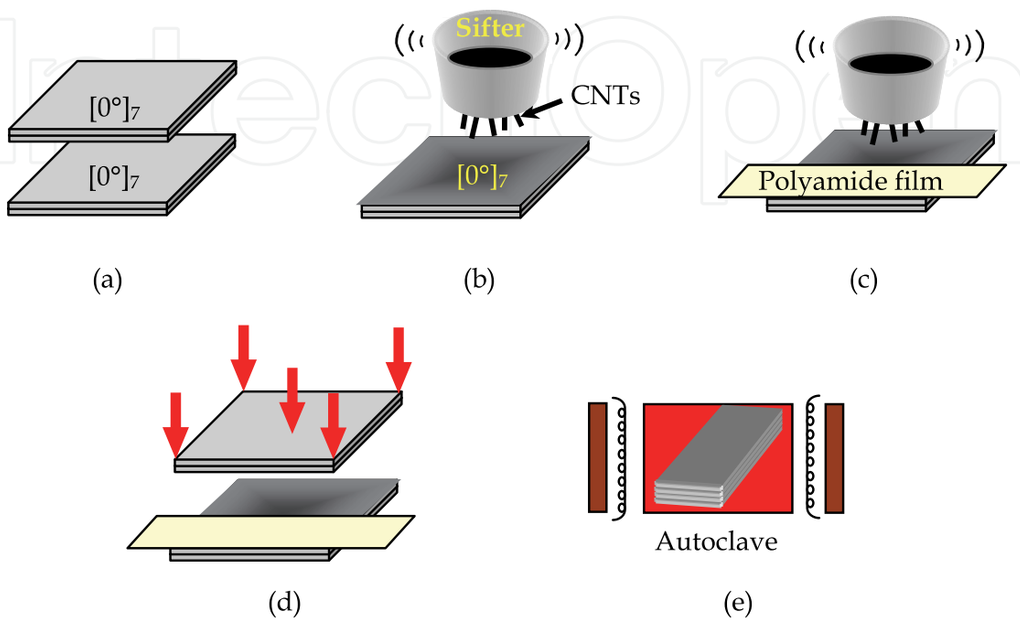

Fig. 2. Powder method

Reinforcement	ρ_A (g/m²)	Notation	t_I (μm)
VGCF®	10	CFRP/VGCF(10)	70
	20	CFRP/VGCF(20)	140
	30	CFRP/VGCF(30)	210
MWCNT-7	5	CFRP/MWCNT(5)	66
	10	CFRP/MWCNT(10)	97
	20	CFRP/MWCNT(20)	148

Table 2. Fabricated hybrid CFRP laminates

2.1.2 DCB test procedure

To evaluate Mode-I interlaminar fracture toughness, DCB tests were carried out using a universal material testing machine (AG-100kNE, Shimazu Co. Ltd, Japan) at 20°C according to Japanese Industrial Standards (JIS K7086). Five specimens for each type were cut from the fabricated laminates, where marked lines were painted on side surface for crack length measurement. The specimens were approximately 20mm wide and 120mm long, with the initial crack of 34mm. The thickness of hybrid CFRP laminates was thicker than that of base CFRP laminates with 3.14mm due to the formed CNTs interlayer. The crosshead speed was 0.5mm/min. Tests were terminated when the increment of crack length Δa reaches 70mm.

2.1.3 Mode-I interlaminar fracture toughness

From the obtained load-COD (crack opening displacement) curves of the above various types of hybrid CFRP laminates, the average critical load at crack growth, i.e. peak load P_c, are plotted in Fig. 3a which shows the obvious increase. The highest P_c occurs at CFRP/VGCF(20) and CFRP/MWCNT(10) , which are about 41% and 17% higher than that of base CFRP laminates, respectively. Obviously, VGCF® performs better than MWCNT-7.

Since P_c is dominated by Mode-I interlaminar fracture toughness G_{IC} and interlaminar tensile strength N, it is anticipated that G_{IC} and N also increase. The average G_{IC} and fracture resistance G_{IR} are demonstrated in Fig. 3b and Fig. 3c. Note that G_{IR} is the average value when the crack length varies from 20mm to 60mm in the obtained R-curves. In Fig. 3b, there are 96% and 58% increase of G_{IC} for CFRP/VGCF(20) and CFRP/VGCF(10), respectively, which can be considered as the optimal addition. In Fig. 3c, CFRP/VGCF(20) has the highest G_{IR}, which is about 25% higher than that of base CFRP laminates. However, the effect of MWCNT on G_{IR} is unpromising. The largest value occurs at CFRP/MWCNT(5) which increases only 6%. Moreover, there is even minor negative influence for some cases on G_{IR}.

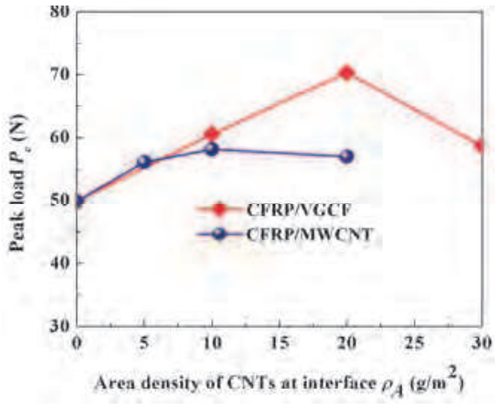

(a) Peak load

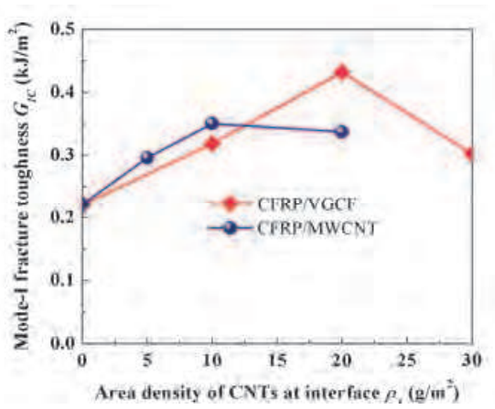

(b) Mode-I fracture toughness

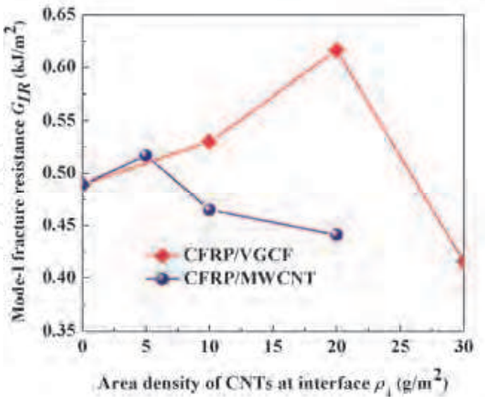

(c) Mode-I fracture resistance

Fig. 3. Reinforcement effects of two commercial CNTs in three-phase hybrid CFRP laminates

The reinforcement mechanism can be explained from crack propagation process observed by an optical microscopy. At the initial stage, crack initiates from crack tip at the CNTs interlayer for all cases (Fig. 4a), which explains the increase of G_{IC}. Moreover, for

CFRP/VGCF(10,20) and CFRP/MWCNT(5), crack extends forward in a zigzag pattern CNTs interlayer (Fig. 4a) creating much more fracture surfaces and consuming much more energy, which leads to the improved G_{IR}. However, for CFRP/VGCF(30) and CFRP/MWCNT(10,20), crack transits from toughened CNTs interlayer toward CFRP plies and propagates forward (Fig. 4c), which results in the decreased G_{IR} compared with that of base CFRP laminates.

(a) CFRP/VGCF(20) (Δa=0mm) (b) CFRP/VGCF(20) (Δa=10mm) (c) CFRP/VGCF(30) (Δa=10mm)

Fig. 4. Crack propagation process for CFRP/VGCF laminates

Moreover, fracture surfaces of DCB specimens were also investigated using scanning electron microscopy (SEM). For CFRP/VGCF(10) and CFRP/MWCNT(5), naked carbon fiber (Fig. 5a) indicates insufficient addition of CNTs at interface. On the other hand, for CFRP/VGCF(30) and CFRP/MWCNT(20), there are obvious defects (Fig. 5c) caused by the poor CNTs dispersion. It explains that CFRP/VGCF(20) and CFRP/MWCNT(10) with good dispersion of CNTs (Fig. 5b) provide best reinforcement effect, respectively.

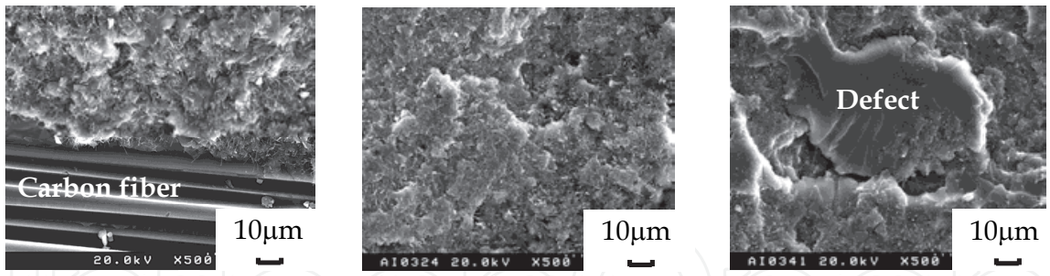

(a) CFRP/VGCF(10) (b) CFRP/VGCF(20) (c) CFRP/VGCF(30)

Fig. 5. Fracture surfaces of CFRP/VGCF laminates

2.2 Numerical simulation using FEM

Instead of experiment, such as butt-joint test under tensile load, FEM simulation on delamination propagation was employed to predict approximately Mode-I interlaminar tensile strength N.

Here, a brick element of 8 nodes [Cao et al., 2002] and a cohesive element [Camanho et al., 2002] were used to model CFRP sublaminates and CNTs interlayer, respectively. The corresponding material properties are listed in Table 3, where the latter was obtained by matching the numerical load-COD curves to experimental ones (see Fig.6). Here, experimental G_{IC} was directly adopted. Interlaminar tensile strength N and initial stiffness K were determined by matching peak load P_c and the initial slope of the numerical load-COD

curves before the peak load, respectively. In Table 3, although N increases with CNTs addition, which are about 75% and 50% higher than that of base CFRP laminates, respectively, there is no any difference among them for different CNTs addition. This can be attributed to that peak load is mainly dominated by G_{IC} while N influences it slightly.
In conclusion, the improvement of interlaminar tensile strength N was confirmed by FEM simulation, and the correctness of experimental G_{IC} was verified from good consistence between numerical and experimental results (Fig.6).

Brick element		**Cohesive element**	N (MPa)	K (N/mm^3)	G_{IC} (kJ/m^2)
E_{11} (GPa)	120	CFRP	20	3.5×10^{-3}	0.221
$E_{22}=E_{33}$ (GPa)	8.8	CFRP/VGCF(10)	35	3.5×10^{-3}	0.318
$G_{12}=G_{13}$ (GPa)	6.0	CFRP/VGCF(20)	35	3.5×10^{-3}	0.432
G_{23} (GPa)	3.7	CFRP/VGCF(30)	35	3.5×10^{-3}	0.302
$\upsilon_{12}=\upsilon_{13}$	0.25	CFFRP/MWCNT(5)	30	3.5×10^{-3}	0.296
υ_{23}	0.45	CFFRP/MWCNT(10)	30	3.5×10^{-3}	0.350
		CFFRP/MWCNT(20)	30	3.5×10^{-3}	0.337

Table 3. Material properties for brick element and cohesive element in FEM simulation

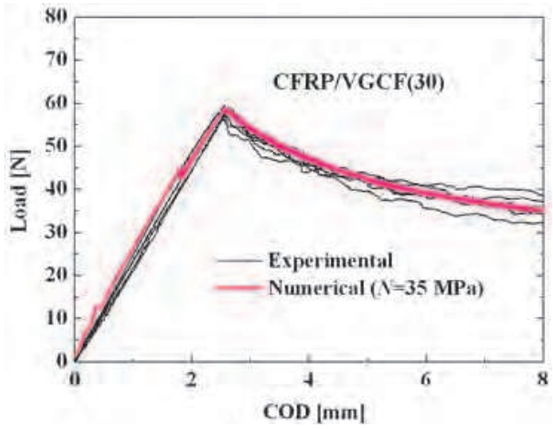

Fig. 6. Comparison of experimental and numerical load-COD curves for CFRP/VGCF(30)

3. Two-phase CNT/Polymer nanocomposites

Pull-out simulations based on MM were carried out to investigate the interfacial properties between CNT and polymer matrix, which were further incorporated into the theoretical model of continuum mechanics to develop a sequential multi-scale model for predicting the overall mechanical properties of two-phase CNT/Polymer nanocomposites. The present method is expected to be applied in CNT-reinforced nanocomposites with various matrices (e.g. metal, ceramics, etc.), which provides useful information for material design.

3.1 Pull-out simulation on Interfacial properties between CNT and polymer matrix

To investigate the interfacial properties between CNT and polymer matrix in two-phase CNT/Polymer nanocomposites only due to van der Waals (vdW) interactions, a series of CNT pull-out simulations from polyethylene (PE) matrix were carried out. Here, the

condensed phase optimization molecular potentials for atomistic simulation studies (COMPASS) force field [Sun, 1998] was employed to calculate the systematic potential energy, which has been broadly testified for CNT itself and CNT-reinforced nanocomposites because of providing reliable results as compared with more accurate tight-binding or ab initio density functional theory based methods. The PE was chosen as matrix because its structural simplicity can effectively reduce the computational cost. Moreover, PE as a representative polymer matrix can give a general picture of the possible interfacial behaviour of various CNT-reinforced polymer nanocomposites. The simulation cell was composed of a fragment of CNT totally embedded inside PE matrix. Taking SWCNT(5,5)/PE nanocomposites as a benchmark, the processes of model building and CNT pull-out are described in detail in the following.

3.1.1 Model building

The unit cell of simulation system, which was of periodic boundary conditions in *y*-*z* plane, was initialized by randomly generating 36 PE chains with initial density of 1.2g/cm^3 surrounding an open-ended SWCNT(5,5). Each PE chain had 20 repeating units of $-CH_2$. The length and diameter of the SWCNT(5,5) fragment were l=4.92nm and D=0.68nm, respectively. Note that the unsaturated boundary effect was avoided by adding hydrogen atoms at both ends of the SWCNT. The hydrogen atom had charge of +0.1268e and the connected carbon atom had charge of -0.1268e, which made the SWCNT neutral. The corresponding computational cell constructed was in the range of 2.69nm×2.69nm×4.9nm in which the volume fraction of SWCNT was V_f=9.0vol.%. Note that the size of computational cell at x axis (i.e. the axial direction of CNT) had to be set large enough to eliminate the interaction among polymer itself [Marietta-Tondin, 2006]. As shown in Fig. 7a, the vacuum layer was set for the CNT pull-out without extending the cell. The size of vacuum layer was about the sum of the cut-off distance of vdW interaction (0.95nm) and nanotube length.

The equilibrated structure of SWCNT/PE nanocomposites in Fig. 7 was obtained as follows:

1. While holding SWCNT as a rigid, by virtue of MD simulations, the model was first put into a constant-temperature, constant-volume (NVT) ensemble for 50ps and then a constant-temperature, constant-pressure (NPT) ensemble for another 50ps with temperature of T=298K, pressure of P=10atm, and time step of Δt=1fs after the initial minimization. The purpose of this step is to slowly compress the structure of the PE to generate an initial amorphous matrix with correct density and low residual stress.
2. The nanocomposite system was further put into NVT ensemble and equilibrated for 50ps at the same time step of Δt=1fs with releasing all rigid constraints on SWCNT. This step is to create a zero initial stress state.
3. Finally, the nanocomposite system was minimized again using MM to obtain the equilibrated configuration in vacuum.

The equilibrated separation distance h between SWCNT and PE matrix due to vdW interaction was about 0.23nm in the present work as shown in Fig. 7b, which is very close to the value of 0.18nm obtained by Han et al. [Han & Elliott, 2007] for SWCNT/PMMA nanocomposites. The difference can be attributed to the different types of polymer.

3.1.2 Pull-out process

The pull-out simulations of SWCNT from PE matrix were carried out by applying displacement-controlled load on the atoms at the right end of CNT. The displacement

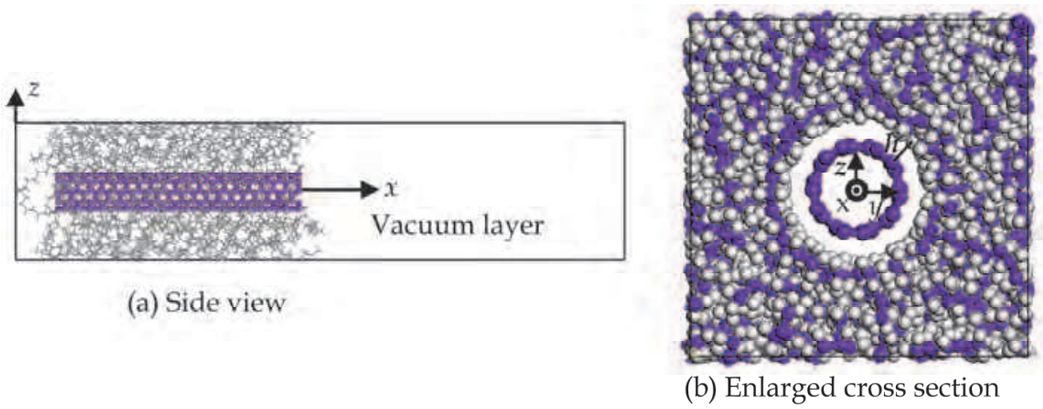

(CNT: l=4.92nm, D=0.68nm, C atoms: purple, H atoms: grey)
Fig. 7. Equilibrated structure of simulation cell for SWCNT(5,5)/PE nanocomposites

increment along the axial (x-axis) direction of CNT was Δx=0.2nm. Snap shots of the atom configurations for SWCNT/PE nanocomposites system during the pull-out process are shown in Fig. 8. Note that the deformation of PE matrix during the pull-out process was neglected by fixing the matrix to reduce the computational cost, since it was confirmed numerically that the influence of the enforced conditions on polymer was very small.
After each pull-out step, the molecular structure was relaxed to obtain the minimum systematic potential energy E by MM. The potential energies of the SWCNT/PE nanocomposites were monitored and recorded during the whole pull-out process, which will be discussed in the following.

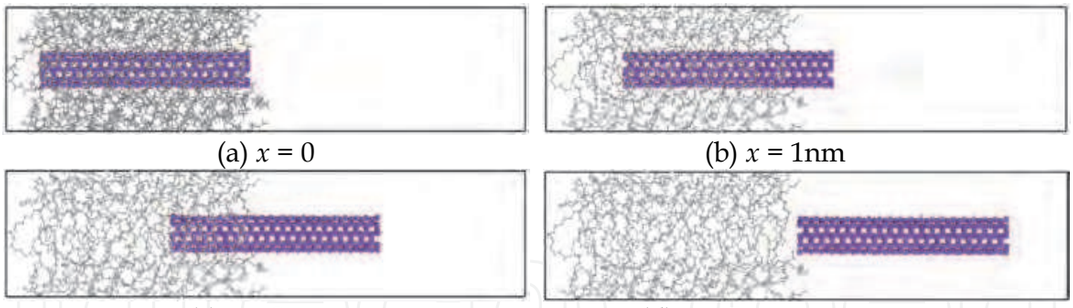

Fig. 8. Snap shots of CNT pull-out from PE matrix

3.1.3 Variation of potential energy during pull-out

In view of that the work done by the pull-out force equals energy increment of nanocomposite system at each pull-out step, the trend of potential energy variation, and the energy increment at each pull-out step becomes very important for analyzing the corresponding pull-out force, and the ISS between CNT and polymer matrix.
The obtained systematic potential energy E during the pull-out is shown in Fig. 9a, which increases gradually accompanied with the CNT pull-out. This trend is just identical to all of the previous simulation results of CNT/Polymer nanocomposites [Liao & Li, 2001; Frankland et al., 2002; Gou et al., 2004; Zheng et al., 2009].

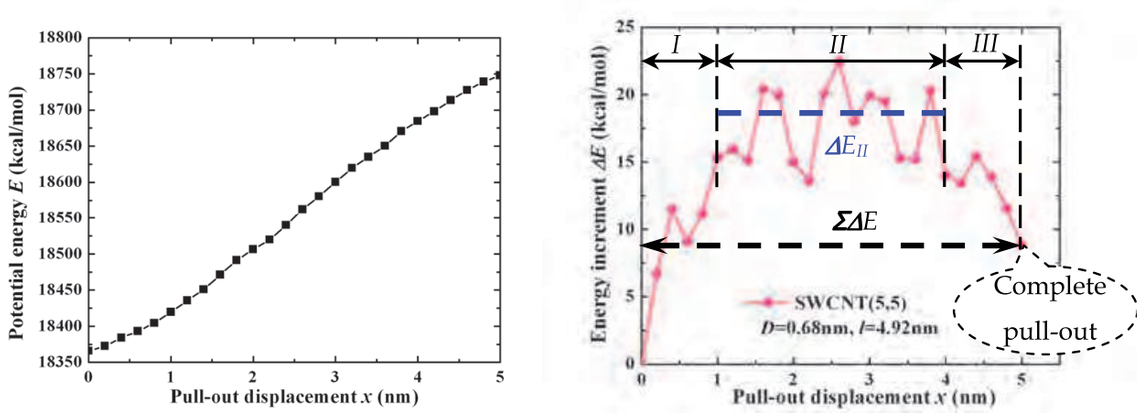

(a) Potential energy E (b) Energy increment $\Sigma\Delta E$

Fig. 9. Variation of E and ΔE during the pull-out of SWCNT(5,5)

Generally, this variation of E can be divided into four parts, i.e. the variation of potential energy in polymer matrix; the variation of potential energy of CNT; the variation of interfacial bonding energy between CNT and polymer matrix; and possible thermal dissipation. Since the polymer was fixed during the pull-out process and the potential energy change of CNT was very small as confirmed in our computations, the variation of E in the present simulation can be mainly attributed to the variation of interfacial bonding energy between CNT and polymer matrix by neglecting thermal dissipation.

Taking an example of the above SWCNT(5,5) pull-out from PE matrix, the calculated energy increment ΔE versus pull-out displacement Δx is shown by pink balls in Fig.9b, where three successive stages can be discerned: in initial stage *I*, ΔE increases sharply; after that, ΔE goes through a long and platform stage *II*, followed by final descent stage *III* until the complete pull-out. As plotted, the total energy change during the pull-out (i.e., the pull-out energy) and the average energy increment in stage *II* are referred to as $\Sigma\Delta E$ and ΔE_{II}, respectively. Moreover, stage *I* and stage *III* have the same approximate range of a=1.0nm which is very close to the cut-off distance of vdW interaction. This trend is surprisingly coincident with that observed sliding behaviour among nested walls in a MWCNT [Li et al., 2010]. The obvious severe fluctuation of energy increment may be attributed to the non-uniformity of polymer matrix in the length direction of CNT. Note that the pull-out energy may also be calculated by using the developed continuum theoretical model for short-fibre reinforced composites (e.g. [Fu & Lauke, 1997]), which plays important role in predicting the fracture toughness of the composites.

On this basis, the effects of CNTs' dimensions on interfacial properties of CNT/Polymer nanocomposites, were explored for the first time by comparing the energy increment of several CNTs with different nanotube length, diameter, or wall number.

3.1.4 Effects of CNTs' dimension

3.1.4.1 Effect of nanotube length

The variation of energy increment corresponding to the pull-out of several SWCNTs(5,5) with different lengths, are plotted in Fig. 10. Just as that in Fig. 9b, three distinct stages are clearly observed for each case. Moreover, among these three curves, there is no obvious

change in the magnitude of the platform stage *II* related to the stable CNT pull-out, which indicates that ΔE_{II} is independent of nanotube length.

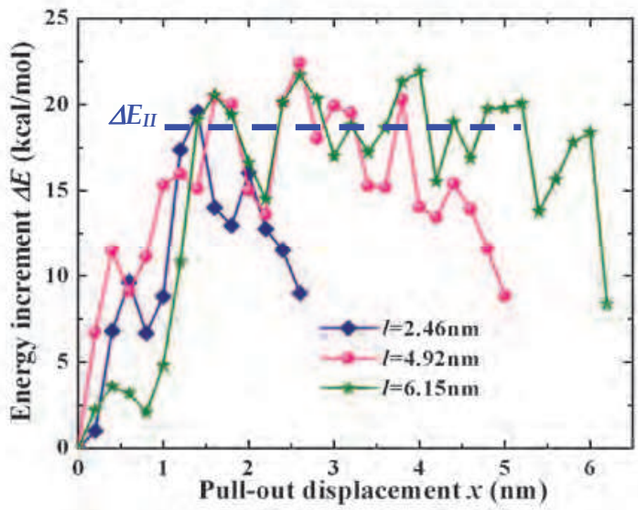

Fig. 10. Effect of nanotube length on energy increment of SWCNT(5,5)

Due to this length-independent behaviour of ΔE_{II}, the length of l_0=3.44nm was employed for all CNTs in the following simulations.

3.1.4.2 Effect of nanotube diameter

The energy increment ΔE corresponding to the pull-out of several SWCNTs with different diameters are illustrated in Fig. 11a, which increases with nanotube diameter. Both $\Sigma\Delta E$ and ΔE_{II} were found to increase linearly with nanotube diameter D as shown in Fig. 11b, which can be fitted as follows:

$$\Sigma\Delta E=277.79D+62.39 \tag{1}$$

$$\Delta E_{II}=19.29\ D+4.27 \tag{2}$$

where D has the unit of nm, $\Sigma\Delta E$ and ΔE_{II} have the unit of kcal/mol. This linear correlation can be explained by the increase of interfacial atoms accompanied with the increase of nanotube diameter. Note that the formula of Eq. (1) for calculating the pull-out energy is only applicable for the pull-out of CNT with the length of l_0=3.44nm, in contrast to the length-independent behaviour of ΔE_{II}. In view of that $\Sigma\Delta E$ increases with nanotube length, for a real SWCNT with length of l_r which is far longer than the present length l_0, $\Sigma\Delta E$ can be estimated as follows

$$\Sigma\Delta E^*=\Sigma\Delta E+\Delta E_{II}\ (l_r-l_0)/\Delta x\ (l_0<l_r) \tag{3}$$

where l_r is of the unit of nm, and the displacement increment here is Δx=0.2nm. Note that $\Sigma\Delta E$ represents the pull-out energy of SWCNT with length of l_0=3.44nm which can be calculated by Eq. (1).

In a word, the average increment in stage *II* (ΔE_{II}) during the pull-out process of the armchair SWCNT from polymer matrix, corresponding to the interfacial properties between CNT and polymer matrix, is independent of nanotube length, but proportional to nanotube

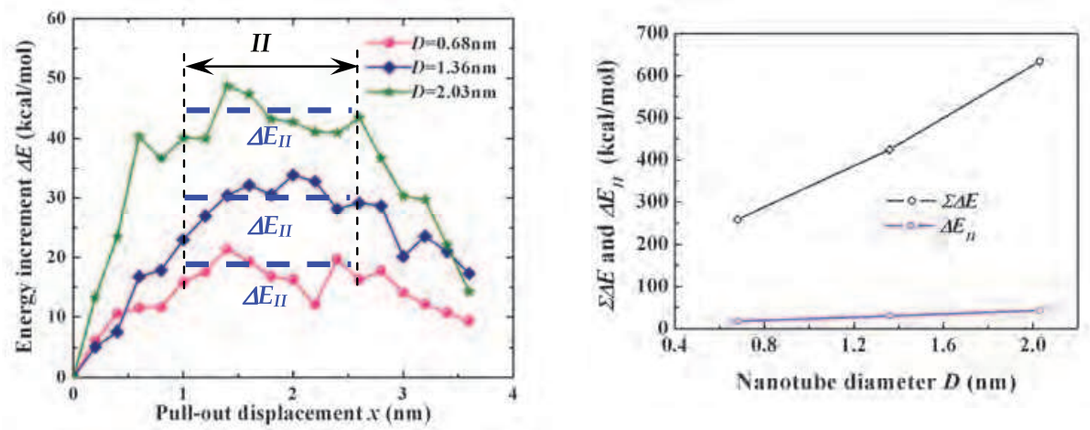

(a) Variation of energy increment (b) Dependence of energy increment on diameter

Fig. 11. Effect of nanotube diameter on energy increment of SWCNT(5,5)

diameter, which is similar to that for the sliding among nested walls in a MWCNT [Li et al., 2010]. Moreover, by using Eqs (1-3), the pull-out energy $\Sigma\Delta E$ and average energy increment in stage *II* ΔE_{II} for the pull-out of any armchair SWCNT can be predicted.

3.1.4.3 Effect of wall number

To investigate the effect of wall number n, three MWCNTs with different wall number were embedded in PE matrix: SWCNT(15,15) with n=1, DWCNT(15,15)/(10,10) with n=2, and TWCNT(15,15)/(10,10)/(5,5) with n=3. The corresponding nanocomposites are referred to as: SWCNT/PE, DWCNT/PE, TWCNT/PE, respectively. Note that the above three CNTs have the same outermost wall with diameter of D_0=2.03nm and length of l_0=3.44nm.

The corresponding energy increment ΔE are plotted in Fig. 12, whose average value in stage *II* (ΔE_{II}) are listed in Table 4. From this table, it can be found that the ΔE_{II} for DWCNT/PE is about 20% higher than that for SWCNT/PE. However, there is only a minor change of ΔE_{II} between DWCNT/PE and TWCNT/PE. The reason can be explained by the increase of distance between newly inserted inner walls and the interface. As the vdW interaction is mostly dependent on the distance, the longer the distance is, the weaker the induced vdW interaction is.

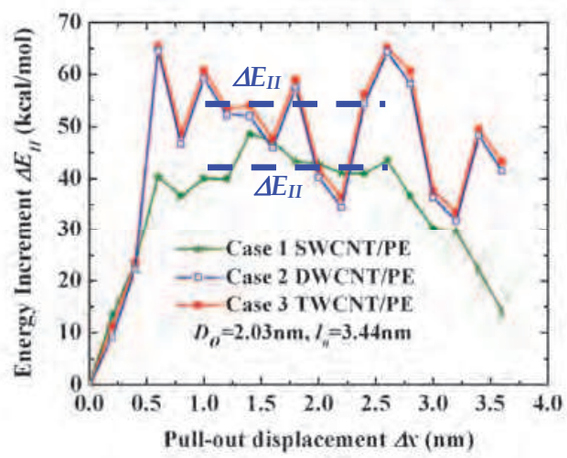

Fig. 12. Effect of n on energy increment

Therefore, ΔE_{II} for the MWCNT ($n \geq 2$) pull-out can be approximately estimated as 1.2 times of that for corresponding SWCNT, which is actually the outermost wall of the MWCNT. To some extent, this finding is consistent with the reports of Schadler [Schadler et al., 1998] who concluded that only the outer walls are loaded in tension for CNT/Epoxy nanocomposites based on the observation of Raman spectrum.
Moreover, the calculated energy increment in the present simulation on the CNT pull-out from polymer matrix is compared with the reports [Li et al., 2010] on the pull-out of outermost wall in the same MWCNT as listed in Table 4. Obviously, the former is smaller than the latter. It may indicate that even for some CNTs with fractured outer walls in the CNT/PE nanocomposites, the CNT is easier to be pulled out from matrix instead of that the fractured outer walls are pulled out against the corresponding inner walls.

	Model	ΔE_{II} (kcal/mol)
CNT Pull-out from PE	SWCNT/PE	43.07
	DWCNT/PE	51.13
	TWCNT/PE	52.71
Pull-out of the outermost wall	DWCNT	55.11
	TWCNT	59.32

Table 4. Comparison of ΔE_{II} for two types of pull-out

3.1.5 Pull-out force

In practical CNT/Polymer nanocomposites, the real pull-out force can be contributed from the following factors [Bal & Samal, 2007; Wong et al., 2003]: vdW interaction between CNT and PE matrix, possible chemical bonding between CNT and PE matrix, mechanical interlocking resulted by local non-uniformity of nanocomposites, such as waviness of CNT, mismatch in coefficient of thermal expansion, statistical atomic defects, etc. Consequently, the pull-out force can be divided into two parts, i.e., $F=F_{vdW}+F_m$. Here, F_{vdW} is the component for overcoming the vdW interaction at the interface which can be calculated by the following Eq. (4); and F_m is the frictional sliding force caused by the other factors stated. The magnitudes of these two parts strongly depend on the interfacial state and CNT dimension. For almost perfect interface, F_{vdW} dominates the pull-out force. On the other hand, for the case of chemical bonding or mechanical interlocking, which in general occurs easily for large CNTs, F_m mainly contributes to the total pull-out force. In the present study, only F_{vdW} and the related ISS for perfect interface are considered as mentioned in the beforehand work.
According to that the work done by the pull-out force at each pull-out step is equal to the energy increment of nanocomposites, the corresponding pull-out force for the stable CNT pull-out stage should be also independent of nanotube length, but proportional to nanotube diameter, just as energy increment is.
From the obtained energy increment ΔE_{II} in Eq. (2) and pull-out displacement increment of Δx=0.2nm, we can get the pull-out force as follows:

$$F_{II} = \Delta E_{II}/\Delta x = \lambda(0.67D+0.15) \tag{4}$$

where F_{II} and D have the units of nN and nm, respectively. The value of λ represents the effect of wall number, which is 1.0 for SWCNT and 1.2 for MWCNT with consideration of the contribution of the inner walls.

3.1.6 Interfacial shear stress (ISS) and surface energy density

Based on the above discussions, the corresponding ISS and surface energy density are analyzed in the following.

The pull-out force is equilibrated with the axial component of vdW interaction which induces the ISS. Conventionally, if we employ the common assumption of constant ISS with uniform distribution along the embedded CNT, the pull-out force F_{II} will vary with the embedded length of CNT, which is obviously contradict with the above length-independent reports of ΔE_{II}. For the extreme case of CNT with infinite length, the ISS tends to be zero, which is physically unreasonable. This indicates that the conventional assumption of ISS is improper for the perfect interface of CNT/PE nanocomposites. Therefore, in view of the above characteristic of the variation of energy increment ΔE_{II}, such as that the range of stage *I* or stage *III* is around 1.0nm, it is concluded that the ISS is distributed solely at each end of embedded CNT within the range of a=1.0nm at the beginning of stage *II* or the end of stage *I*. In view of the dependence of vdW force upon the distance between two atoms, the ISS at each end of the embedded CNT which is induced by the variation of vdW force, should at first increase sharply and then decrease slowly to zero after reaching the maximum. Here, by assuming its uniform distribution within two end regions for simplicity, the effective ISS can be derived as

$$\tau_{II} = F_{II}/(2\pi Da) \tag{5}$$

By using Eqs. (1-5), the pull-out energy $\Sigma\Delta E$, the average pull-out force F_{II} and the ISS τ_{II} for CNT/PE nanocomposites can be calculated. As shown in Fig. 13a, the calculated ISS is found to decrease initially with nanotube diameter and saturate at the value of 106.7MPa for SWCNT/PE nanocomposites. For MWCNT/PE, the saturated value is 128MPa, which is about 1.2 times of that for SWCNT/PE, both of which has the same outermost wall.

On the other hand, in view of that two new surface regions are generated at the two ends of CNT after each pull-out step, the corresponding surface energy should be equal to the energy increment ΔE_{II} by neglecting thermal dissipation. Therefore, the surface energy density can be calculated as

$$\gamma_{II} = \Delta E_{II}/(2\pi D\Delta x) = F_{II}/(2\pi D) \tag{6}$$

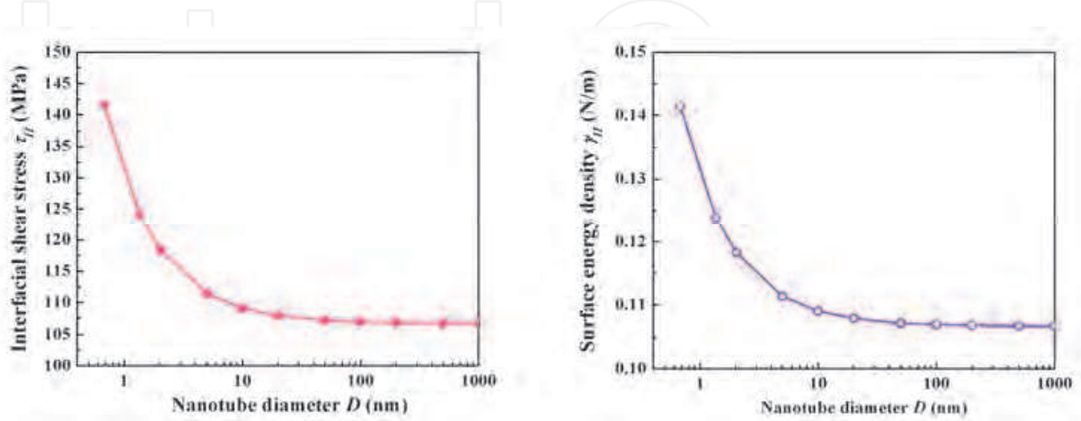

(a) Interfacial shear stress (ISS) (b) Surface energy density

Fig. 13. Dependence of ISS and surface energy density on nanotube diameter

As shown in Fig. 13b, the surface energy density has the same trend as the ISS, which initially decreases slightly as nanotube diameter increases and finally converges at the value of 0.11N/m. This value is very close to the previous reports of 6-8meV/Å² (i.e., 0.09-0.12N/m) [Lordi & Yao, 2000] and 0.15 kcal/molÅ² (i.e., 0.1 N/m) [Al-Ostaz et al., 2008] for SWCNT/PE nanocomposites, which indicates the effectiveness of the present simulation.

3.1.7 Comparison with previous reports

The predicted ISS in the present study as given in Table 5 is obviously higher than that in the previous reports [Frankland et al., 2002; Zheng et al., 2009; Al-Ostaz et al.] which is calculated from

$$\tau^{*}=2\Sigma\Delta E/(\pi D l^{2}) \tag{7}$$

The reason of this big difference is that the assumption of the constant ISS with uniform distribution along the total embedded length of CNT employed in previous numerical simulation, which has been verified to be unreasonable here.

Ref.	SWCNT		Experimental reports		Present prediction	
	D (nm)	l (nm)	$\Sigma\Delta E^{*}$ (kcal/mol)	τ^{*} (MPa)	$\Sigma\Delta E^{*}$ (kcal/mol)	τ_{II} (MPa)
[Frankland et al., 2002]	1.36	5.3	×	2.7	707.4	123.9
[Zheng et al., 2009]	1.36	5.9	~500	33	798.8	123.9
[Al-Ostaz et al., 2008]	0.78	4.2	224	133	352.2	137

Table 5. Prediction in previous simulations for SWCNT/PE nanocomposites

For the pull-out force, the calculated values using the proposed formulae of Eqs.(1-4) are compared with that reported in direct CNT pull-out experiments at nano-scale from several different polymer matrices, as shown in Table 6. Obviously, the reported pull-out forces are much higher than the calculated values only when vdW interactions are considered at the interface between CNT and polymer matrix, although severe experimental data scattering has been observed which may be caused by manipulation process or force/displacement measurement. The reason can be attributed to the following factors.

Firstly, if we take into account the curvature of CNT (Fig. 14a), the necessary pull-out force will increase. Considering a special case with the highest probability where an inclined angle θ between the axial direction of CNT and the pull-out direction is 45° (Fig. 14b), the

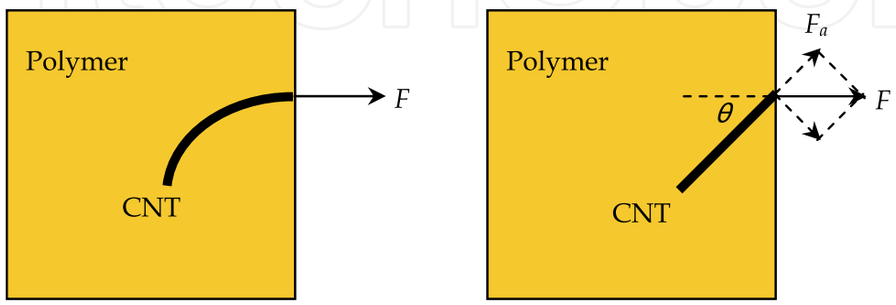

(a) Curved CNT (b) Oblique CNT

Fig. 14. Simplified model for the pull-out of curved and oblique CNT

Ref.	Matrix	MWCNT	Pull-out force (μN)	
		D (nm)	Exp.	Prediction
[Deng, 2008]	PEEK	49	1.04	0.04
		89	8.6	0.07
[Barber et al., 2003]	PE-butene	80	0.85	0.07
[Cooper et al., 2002]	Epoxy	8.2	3.8	0.01
		11	2.8	0.01
		13.4	0.6/2.3	0.01
		24	6.8/12.8	0.2

Table 6. Prediction of previous experiments for MWCNT/Polymer nanocomposites

corresponding pull-out force will increase about 40%. By observing the data in Table 6, this increase effect is still too small compared with the experimental data.

Secondly, for the effect of the pressure or residual stress in nanocomposites, a simple representative volume element (RVE) model (Fig. 15a) was constructed to perform FEM analysis. This continuum mechanics based computation is valid, at least qualitatively when the diameter of CNT is over several tens of nanometers. Assuming the symmetrical structure, the quarter part of interface region (i.e. the blue part in Fig. 15b) was employed.

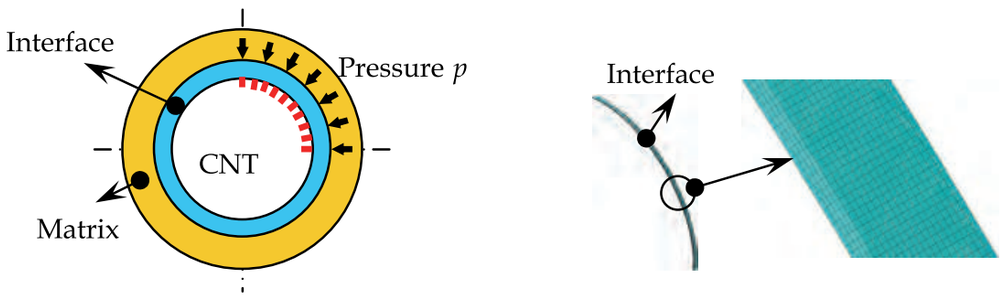

(a) Simplified composite model (b) FEM model of interface

Fig. 15. Simplified FEM model of interface between CNT and matrix

The inner wall surface of the interface region was fixed as boundary condition, which represents the rigid CNT. The uniform static pressure was applied on the outer wall of interface region. Two values of Young's modulus E_i for the interface region were considered, i.e., 1GPa and 3GPa. The corresponding FEM model is shown in Fig. 15b, where the size of element size was taken as 0.05nm for convergence and accuracy.

The relationship of strain energy density γ and the applied pressure p is shown in Fig. 16, in which strain energy increases by the power of square with p. It can be found that a large pressure p can only cause very small increase of strain energy density γ, which indicates that the effect of pressure or residual stress is not as strong as we expected. In general, the residual stress in polymer nanocomposites ranges from 25.0MPa to 40.0MPa. For instance, for the case of E_i=1GPa of interface region, by applying for the pressure of 30.0MPa, the strain energy density is around 2.85×10^{-5}N/m, which is still much smaller than the surface energy density of γ_{II}=0.11N/m caused by vdW interaction as stated previously. It means that the pressure or residual stress in polymer nanocomposite system is not a dominant factor.

The above discussion leads to an important conclusion, i.e., the interface properties between CNT and polymer matrix contributed by vdW interaction is quite minor for the real

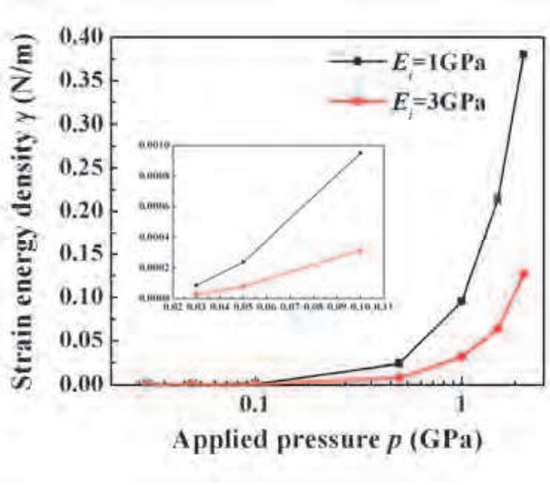

Fig. 16. Relationship between applied pressure and strain energy density

CNT pull-out from polymer matrix. Therefore, to accurately evaluate the interfacial properties for real case, it is necessary to incorporate the effects of frictional sliding caused by mechanical interlocking, atomic statistical defects, or chemical bonding. Moreover, for effectively improving the interfacial properties and therefore the mechanical properties of bulk nanocomposites, it is vital to incorporate into chemical bonding and mechanical interlocking, which will be the topic in the future.

Note that although the type of polymer will influence the value of ISS which is not discussed in the present work, the characteristics of pull-out force and the corresponding ISS will be similar to those discussed in CNT/PE nanocomposites here.

3.2 Characterization on overall mechanical properties of CNT/Polymer nanocomposites

To investigate the overall mechanical properties of CNT/Polymer nanocomposites, tensile tests and SENB tests were carried out, in which MWCNT-7 and VGCF® were used as reinforcement filler, respectively. Moreover, a sequential multi-scale model was developed by incorporating the interfacial properties between CNT and polymer matrix obtained from previous pull-out simulations into the conventional continuum theory, which connects the interfacial properties to overall mechanical properties of CNT/Polymer nanocomposites.

3.2.1 Mechanical tests for CNT/Epoxy nanocomposites

Epoxy resin jER806 (Japan Epoxy Resins Co., Ltd., Japan) and the hardener Tohmide-245LP (Fuji Kasei Kogyou Co., Ltd., Japan) were used to prepare the polymer matrix with the weight ration of 100:62. According to the weight fraction W_f of reinforcements, two groups of nanocomposites were fabricated: MWCNT/Epoxy with W_f of MWCNT-7 varying at 2, 3, 4%, and VGCF/Epoxy with W_f of VGCF® varying at 2, 4, 6%. The fabrication process as shown in Fig. 17 is described below:

1. The epoxy resin was first heated to 60˚C in an oven to decrease the viscosity for its better miscibility with MWCNTs;
2. Then the CNTs were dispersed into the epoxy resin using the planetary centrifugal mixer at 2000rpm for 10min;

3. After adding the hardener, the mixture was agitated for another 10 min at 1000rpm;
4. Subsequently, the mixture was poured into the silicon mould for a pre-curing process with 12h at room temperature, followed by a post-curing process which was performed at 80˚C in the oven for 6h.

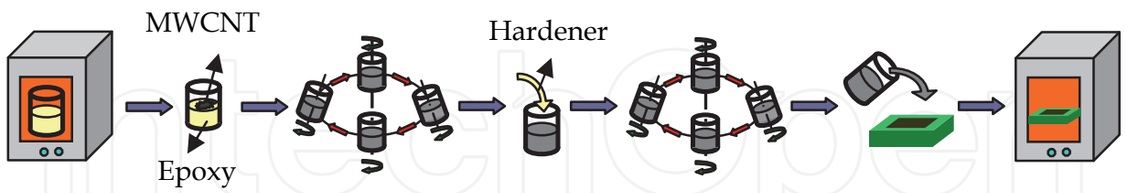

Fig. 17. Fabrication of MWCNT/Epoxy nanocomposites for mechanical tests

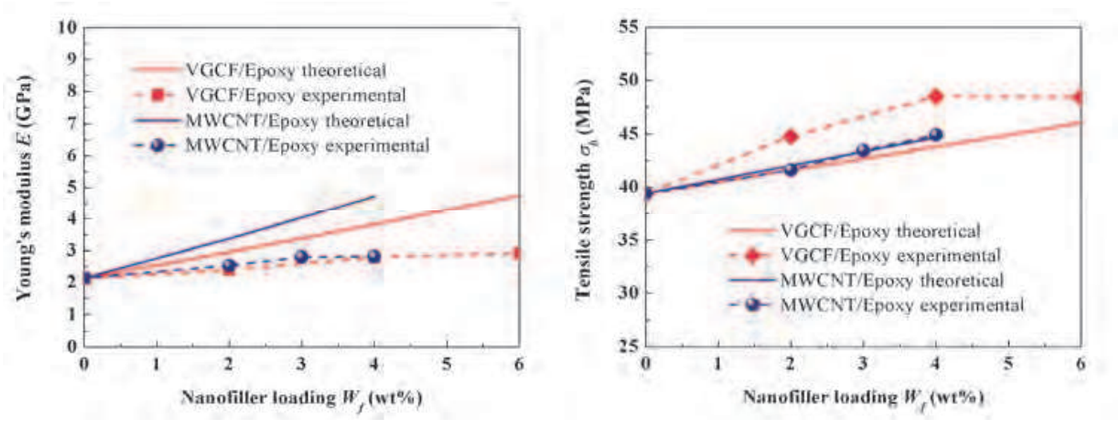

(a) Young's modulus (b) Tensile strength

Fig. 18. Comparison of theoretical and experimental Young's modulus and tensile strength

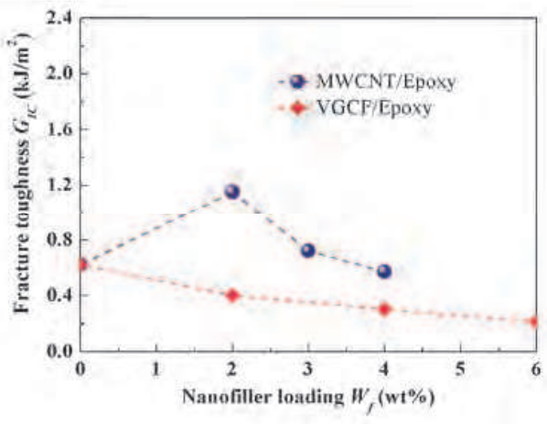

Fig. 19. Experimental fracture toughness

According to ASTM D638 (Type V) and ASTM D5045 standards, tensile tests and SENB tests were preformed. Three specimens of the above fabricated composites at a specified CNT loading were prepared. A universal materials testing machine (Instron 5567) was used with

a cross-head speed of 0.25mm/min. The Poisson's ratio of nanocomposites measured in tensile tests by using bi-axial strain gages was directly used in the evaluation of fracture toughness in SENB tests.

The obtained Young's modulus E_c, tensile strength σ_c of MWCNT/epoxy and VGCF/Epoxy nanocomposites are plotted in Fig. 18. As shown in Fig. 18a, the largest increase of 31% and 36% in E_c from 2.14GPa of neat epoxy occur at 4wt% loading for MWCNT/Epoxy and at 6wt% loading for VGCF/Epoxy, respectively. In Fig. 18b, σ_c increases obviously for nanocomposites. At 4wt% loading, the highest increases are 14.1% for MWCNT/Epoxy and

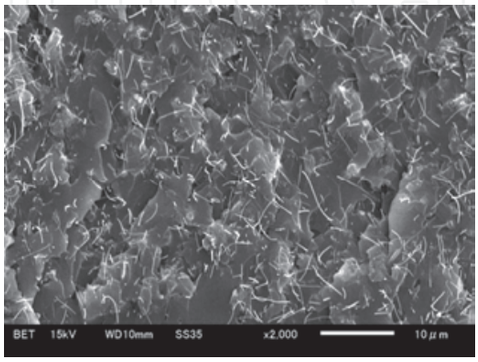

(a) MWCNT/Epoxy (3wt%)

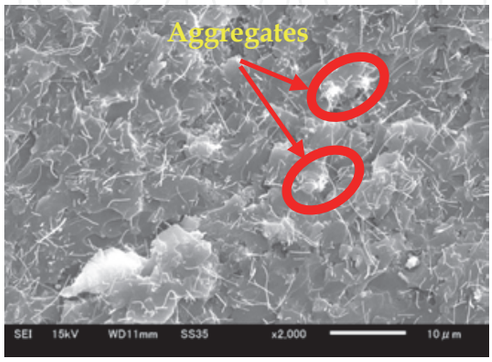

(b) MWCNT/Epoxy (4wt%)

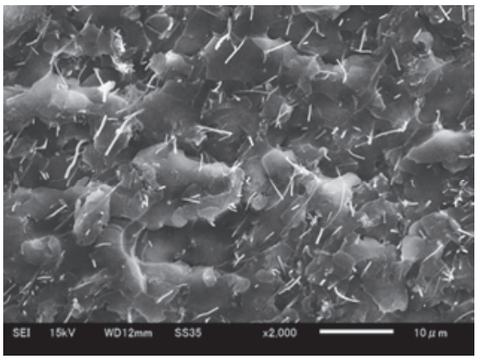

(c) VGCF/Epoxy (4wt%)

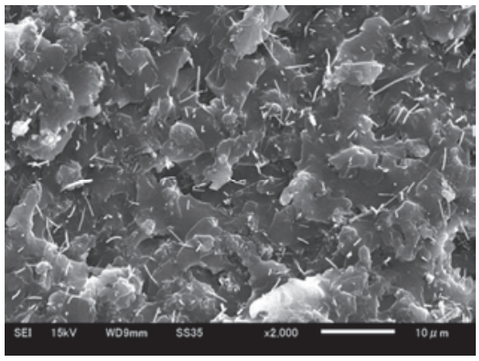

(d) VGCF/Epoxy (6wt%)

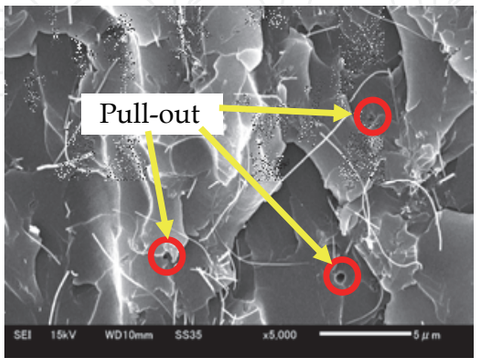

(e) MWCNT/Epoxy (2wt%)

Fig. 20. SEM pictures of SENB specimens

23.1% for VGCF/Epoxy from 39.4MPa of neat epoxy. The effect of VGCF in σ_c is slightly better than that of MWCNT. Moreover, σ_c decreases slightly when the addition is over 4wt% for VGCF/Epoxy. However, there is no obvious saturation trend in σ_c even at 4wt% loading of MWCNT, which means that σ_c may be enhanced with further addition of MWCNT. The corresponding Mode-I fracture toughness G_{IC} is given in Fig. 19, a remarkable increase, i.e. 85.5% can be identified for 2wt% MWCNT loading, although the effect of VGCF to G_{IC} is unpromising.

In order to clarify the reinforcement mechanism, SEM observations were performed on the fracture surfaces of SENB specimens as shown in Fig. 20. Even there are some small aggregates at a high loading, e.g. 4wt% in Fig. 20(b), good dispersion of MWCNT or VGCF can be identified, which leads to the increase of E and σ_b in both nanocomposites. As shown in Fig. 19, 6wt% VGCF leads to the lowest G_{IC} while 2wt% MWCNT provides the highest G_{IC}. However, it is difficult to distinguish them through the fracture surfaces from Fig. 20 (d) and (e), although the former demonstrates a clear brittle fracture feature. One possible reason for the increase of G_{IC} in 2wt% MWCNT may be there are more pull-out holes of MWCNT, which improves the fracture toughness.

3.2.2 Theoretical prediction on tensile properties of MWCNT/Polymer nanocomposites

With consideration of fibre length and fibre orientation distribution, Cox's shear-lag model [Cox, 1952; Krenchel, 1964] predicts the longitudinal modulus of short-fiber reinforced composites as

$$E=\eta_o\eta_l E_f V_f+E_m(1-V_f) \tag{8}$$

where V_f is the volume fraction of fiber, E_f and E_m are Young's moduli of nanofiller and matrix, respectively. The orientation efficiency factor η_o is 1/5 for three-dimensional random distribution, and the nanofiller length efficiency factor η_l was given in Ref. [Cox, 1952]. The predicted Young's modulus is also plotted in Fig. 18(a), which is a bit higher than experimental ones, especially for higher nanofiller loadings, which may be caused by the difficult dispersion of nanofiller in experiments.

For short-fiber reinforced composites under the assumption of iso-strain state in the fibers and matrix, Fukuda and Chou [Fukuda & Chou, 1982] developed a probabilistic theory as follows

$$\sigma_{ultc}=\begin{cases}\sigma_{ultf}V_f\left(1-\dfrac{l_c}{2l_f}\right)C_0+\sigma_m'\left(1-V_f\right) & (l>l_c)\\ \sigma_{ultf}V_f\left(\dfrac{l_f}{2l_c}\right)C_0+\sigma_m'\left(1-V_f\right) & (l\le l_c)\end{cases} \tag{9}$$

where l_f is the length of fiber, σ_{ultf} the tensile strength of fiber, σ_m' the matrix stress at the failure of composites, and C_0 the orientation factor which is 1/8 in the case of three-dimensional random array model. The critical length l_c is defined as [Kelly & Tyson, 1965]

$$l_c=\sigma_{ultf}r_f V_f/\tau_y \tag{10}$$

where r_f is the fiber radius, and τ_y is the shear strength of fiber/matrix interface.

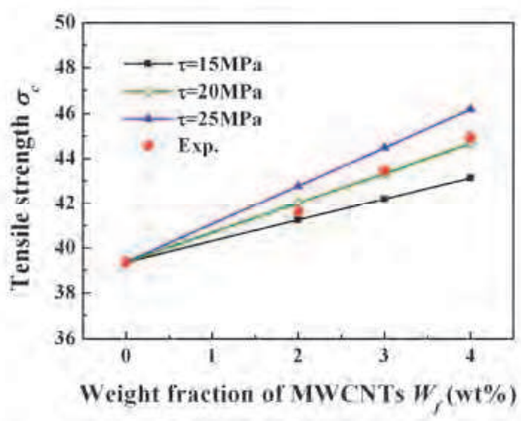

Fig. 21. Prediction of σ_c for MWCNT/Epoxy

Here, the key point is how to define the shear strength τ_y by using the previous MM simulation results. With consideration of its distribution which is only at each end of embedded CNT within 1.0nm, the shear strength should be around 106.7MPa for SWCNT, and 128.04MPa for MWCNT which is about 1.2 times of that for SWCNT. On the other hand, if we define the shear strength based on the whole embedded length of CNT (e.g., 5μm for present experiments), the corresponding shear strength can be calculated as 0.09MPa for SWCNT, and 0.1MPa for MWCNT. Naturally, these values defined from the conventional conception of shear strength seem to be very small from common sense. It further confirms the previous analysis, which indicates that the contribution from vdW interaction to the pull-out force may be comparatively small in practical nanocomposites compared with that from frictional sliding caused by possible chemical bonding or mechanical interlocking. From the above statements, no matter what kind of definition for the shear strength is used, the interfacial shear strength can be assumed to range from 0.1MPa to 128.04MPa for MWCNT. Naturally, by considering the obliqueness of CNT (Fig.14) to the direction of pull-out force, this shear strength range can modified as 0.14~179.26MPa. With consideration of the effects of residual stress in polymer systems, and especially possible chemical bonding or mechanical interlocking, the above range may be increased significantly. Taking the possible range of 0.5~200MPa, the corresponding critical length is about 9750 ~24.38μm, all of which are much longer than that of the MWCNTs used, i.e. $l_f \ll l_c$. It means that the reinforcement effect predicted theoretical in Eq. (7) is unpromising. Replacing $\sigma_m^{'}$ by the measured tensile strength of neat epoxy σ_m, the tensile strength of MWCNT/Epoxy nanocomposites can be predicted. As shown in Fig. 21, the interfacial shear strength of 15~25MPa provides good consistence between experimental measurements and theoretical prediction. Therefore, the previously stated wide range for ISS can rightly cover this narrow band, which indicates that the present multi-scale method is meaningful. Moreover, if we employ the conventional definition of interfacial shear strength which leads to a value lower than 1MPa, it is obviously lower than 15~25MPa. This indicates that the contribution from frictional sliding dominates the interfacial shear strength, which is at least 10 times higher than that from vdW interaction. Taking the value of 20MPa for interfacial shear strength, the predicted value is plotted in Fig. 18b, which indicates good consistence with experimental results.

4. Conclusion

The above research results clearly clarify the different reinforcement effects of two kinds of CNTs (i.e., MWCNT-7 and VGCF®) in two types of nanocomposites (i.e., three-phase hybrid CFRP laminates and two-phase CNT/Polymer nanocomposites).

For **three-phase hybrid CFRP laminates**, a new simple fabrication method *powder method* was developed to disperse CNTs at the interface between CFRP plies. DCB experiments and FEM analysis were carried out which verifies the significant improvement of interlaminar mechanical properties.

For **two-phase CNT/Polymer nanocomposites**, the interfacial properties between CNT and polymer matrix was clarified, where the effects of nanotube length, diameter and wall number were explored for the first time. Moreover, the obtained interfacial mechanical properties were incorporated into the continuum mechanics to develop a sequential multi-scale model, which predicts the overall mechanical properties of nanocomposites and indicates the relationship between the interfacial properties and overall mechanical properties.

5. Acknowledgment

This work is partly supported by two Grand-in-Aids for Scientific Research (No. 19360045 and No. 22360044) from the Japanese Ministry of Education, Culture, Sports, Science and Technology. The authors acknowledge Prof. C. B. Fan (Beijing Institute of Technology, China) for kindly providing the computational resources.

6. References

Ajayan, P.M.; Stephan, O.; Colliex, C. & Trauth, D. (1994) Aligned Carbon Nanotube Arrays Formed by Cutting a Polymer Resin-nanotube Composite. *Science,* Vol. 265, pp 1212.

Al-Ostaz, A.; Pal, G.; Mantena, P.R.; Cheng, A. (2008) Molecular Dynamics Simulation of SWCNT-Polymer Nanocomposite and its Constituents. *Journal of Materials Science,* Vol. 43, pp 164-173.

Andrews, R.; Jacques, D.; Minot, M. & Rantell, T. (2002) Fabrication of Carbon Multiwall Nanotube/Polymer Composites by Shear Mixing. *Macromolecular Materials and Engineering,* Vol. 287, pp 395-403.

Arai, M.; Noro, Y.; Sugimoto, K. & Endo M. (2008) Mode I and Mode II Interlaminar Fracture Toughness of CFRP Laminates Toughened by Carbon Nanofiber Interlayer. *Composites Science and Technology,* Vol. 68, pp 516-525.

Bal, S. & Samal, S.S. (2007) Carbon Nanotube Reinforced Polymer Composites - A State of Art. *Bulletin of Materials Science,* Vol. 30, No. 4, pp 379-386.

Bangarusampath, D.S.; Ruckdaschel, H.; Altstadat, V.; Sandler, J.K.W.; Garray, D.& Shaffer M.S.P. (2009) Rheology and Properties of Melt-Processed Poly (ether ether ketone)/ Multi-Wall Carbon Nanotube Composites. *Polymer,* Vol. 50, pp 5803- 5811.

Barber, A.H.; Cohen, S.R.; Kenig, S. & Wagner, H.D. (2003) Measurement of Carbon Nanotube-Polymer Interfacial Strength. *Applied Physics Letters,* Vol. 82, No. 23, pp 4140-4142.

Barber, A.H.; Cohen, S.R.; Kenig, S. & Wagner, H.D. (2004) Interfacial Fracture Energy Measurements for Multi-walled Carbon Nanotubes Pulled from a Polymer Matrix. *Composite Science and Technology,* Vol. 64, pp 2283-2289.

Bhattacharyya, A.R.; Sreekumar, T.V.; Liu, T.; Kumar, S.; Ericson, L.M.; Hauge, R.H. & Smalley, R.E. (2003) Crystallization and Orientation Studies in Polypropylene/Single Wall Carbon Nanotube Composite. *Polymer,* Vol. 44, pp 2373-2377.

Camanho, P.P. & Davila, C.G. (2002) Mixed-mode Decohesion Finite Elements for the Simulation of Delamination in Composite Materials. NASA/TM, pp. 211737.

Cao, Y.; Hu, N.; Lu, J.; Fukunaga, H. & Yao, Z. (2002) A 3D Brick Element based on Hu-Washizu Variational Principle for Mesh Distortion. *International Journal for Numerical Methods in Engineering,* Vol. 53, pp 2529-2548.

Chowdhury, S.C. & Okabe, T. (2007) Computer Simulation of Carbon Nanotube Pull-out from Polymer by the Molecular Dynamics Method. *Composites Part A,* Vol. 38, pp 747-754.

Chang, T.E.; Jensen, L.R.; Kisliuk, A.; Pipes, R.B.; Pyrz, R. & Sokolov, A.P. (2005) Microscopic Mechanism of Reinforcement in Single-Wall Carbon Nanotube/Polypropylene Nanocomposite. *Polymer,* Vol. 46, pp 439-444.

Chang, T.E.; Kisliuk, A.; Rhodes, S.M.; Brittain, W.J. & Sokolov, A.P. (2006) Conductivity and Mechanical Properties of Well-Dispersed Single-Wall Carbon Nanotube/ Polystyrene Composite. *Polymer,* Vol. 47, pp 7740-7746.

Ci, L. & Bai, J. (2006) The Reinforcement Role of Carbon Nanotues in Epoxy Composites with Different Matrix Stiffness. *Composite Science and Technology,* Vol. 66, pp 599-603.

Cooper, C.A.; Ravich, D.; Lips, D.; Mayer, J. & Wagner, H.D. (2002) Distribution and Alignment of Carbon Nanotubes and Nanofibrils in a Polymer Matrix. *Composite Science and Technology,* Vol. 62, pp 1105-1112.

Cooper, C.A.; Cohen, S.R.; Barber, A.H. & Wagner, H.D. (2002) Detachment of Nanotubes from a Polymer Matrix. *Applied Physics Letters,* Vol. 81, No. 20, pp 3873-3875.

Cox, H.L. (1952) The Elasticity and Strength of Paper and Other fibrous Materials. *British Journal of Applied Physics,* Vol. 3, pp 72-79.

Curran, S.; Davey, A.P.; Coleman, J.; Dalton, A.; McCarthy, B.; Maier, S.; Drury, A.; Gray, D.; Brennan, M.; Ryder, K.; Chapelle, M.L.; Journet, C.; Bernier, P.; Byrne, H.J.; Carroll, D.; Ajayan, P.M.; Lefrant, S.; Blau, W. (1999) Evolution and Evalution of the Polymer/Nanotube Composite. *Synthetic Metals,* Vol. 103, pp 2559-2562.

Demczyk, B.G.; Wang, Y.M.; Cumings, J.; Hetman, M.; Han, W.; Zettl, A.; Ritchie, R.O. (2002) Direct Mechanical Measurement of the Tensile Strength and Elastic Modulus of Multiwalled Carbon Nanotubes. *Materials Science and Engineering A,* Vol. 334, pp 173-178.

Deng, F.; Ogasawara, T. & Takeda, N. (2007) Experimental Characterization of Poly (Ether Ether Ketone)/Multi-Wall Carbon Nanotube Composites. *Key Engineering Materials,* Vol. 334-335, pp 721-724.

Deng, F. (2008) Investigation of the Interfacial Bonding and Deformation Mechanism of the Nano Composites Containing Carbon Nanotubes. Tokyo University. PhD Dissertation.

Ding, W.; Eitan, A.; Fisher, FT.; Chen, X.; Dikin, D.A.; Andrews, R.; Brinson, L.C.; Schadler, L.S. & Ruoff, R.S. (2003) Direct Observation of Polymer Sheathing in Carbon Nanotube-Polycarbonate Composites. *Nano Letters,* Vol. 3, No. 11, pp 1593-1597.

Frankland, S.J.V.; Caglar, A.; Brenner, D.W. & Griebel, M. (2002) Molecular Simulation of the Influence of Chemical Cross-links on the Shear Strength of Carbon Nanotube-Polymer Interfaces. *Journal of Physical Chemistry B,* Vol. 106, pp 3046-3048.

Fu, S.Y. & Lauke, B. (1997) The Fiber Pull-out Energy of Misaligned Short Fibre Composites. *Journal of Materials Science,* Vol. 32, pp 1985-1993

Gao, X.L. & Li, K. (2005) A Shear-lag Model for Carbon Nanotube-Reinforced Polymer Composites. *International Journal of Solids and Structures,* Vol. 42, pp 1649- 1667.

Garcia, E.J.; Wardle, B.L. & Hart, A.J. (2008) Joining Prepreg Composite Interfaces with Aligned Carbon Nanotubes. *Composites Part A,* Vol. 39, pp 1065-1070.

Gojny, F.H.; Nastalczyk, J.; Roslaniec, Z. & Schulte, K. (2003) Surface Modified Multi-Walled Carbon Nanotubes in CNT/Epoxy-Composites. *Chemical Physics Letters,* Vol. 370, pp 820-824.

Gojny, F.H.; Wichmann, M.H.G.; Fiedler, B. & Schulte, K. (2005) Influence of Different Carbon Nanotubes on the Mechanical Properties of Epoxy Matrix Composites - A Comparative Study. *Composite Science and Technology,* Vol. 65, pp 2300- 2313.

Gojny, F.H.; Wichmann, M.H.G.; Kopke, U.; Fiedler, B. & Schulte, K. (2004) Carbon Nanotube-Reinforced Epoxy-Composites: Enhanced Stiffness and Fracture Toughness at Low Nanotube Content. *Composite Science and Technology,* Vol. 64, pp 2363-2371.

Gou, J.; Minaie, B.; Wang, B.; Liang, Z. & Zhang, C. (2004) Computational and Experimental Study of Interfacial Bonding of Single-walled Nanotube Reinforced Composites. *Computational Materials Science,* Vol. 31, pp 225-236.

Haggenmueller, R.; Gommans, H.H.; Rinzler, A.G.; Fischer, J.E. & Winey, K.I. (2000) Aligned Single-wall Carbon Nanotubes in Composites by Melt Processing methods. *Chemical Physics Letters,* Vol. 330, No.10, pp 219-225.

Han, Y. & Elliott, J. (2007) Molecular Dynamics Simulations of the Elastic Properties of Polymer/Carbon Nanotube Composites. *Computational Materials Science,* Vol. 39, No. 2, pp 315-323.

He, X.; Zhang, F.; Wang, R. & Liu, W. (2007) Preparation of a Carbon Nanotube/Carbon Fiber Multi-Scale Reinforcement by Grafting Multi-walled Carbon Nanotubes onto the Fibers. *Carbon,* Vol. 45, pp 2559-2563.

Inam, F.; Wong, D.W.Y.; Kuwata, M. & Peijs, T. (2010) Multiscale Hybrid Micro-Nanocomposites based on Carbon Nanotubes and Carbon Fibers. *Journal of Nanomaterials.* (In press)

Jiang, X.; Bin, Y. & Matsuo M. (2005) Electrical and Mechanical Properties of Polyimide-Carbon Nanotubes Composites Fabricated by In Situ Polymerization. *Polymer,* Vol. 46, pp 7418-7424.

Jiang, L.Y.; Huang, Y.; Jiang, H.; Ravichandran, G.; Gao, H.; Hwang, K.C. & Liu, B. (2006) A Cohesive Law for Carbon Nanotube/Polymer Interfaces based on the van der Waals Force. *Journal of the Mechanics and Physics of Solids,* Vol. 54, pp 2436- 2452.

Jin, L.; Bower, C. & Zhou, O. (1998) Alignment of Carbon Nanotube in a Polymer Matrix by Mechanical Stretching. *Applied Physics Letters,* Vol. 73, No. 9, pp1197-1193.

Karapappas, P.; Vavouliotis, A.; Tsotra, P. & Kostopoulos, V. (2009) Enhanced Fracture Properties of Carbon Reinforced Composites by the Addition of Multi-Wall Carbon Nanotubes. *Journal of Composite Materials,* Vol. 43, No. 9, pp 977-985.

Kelly, A. & Tyson, W.R. (1965) Tensile Properties of Fiber-reinforced Metals: Copper/Tungsten and Copper/Molybdenum. *Journal of the Mechanics and Physics of Solids,* Vol. 13, pp 329-350.

Kepple, K.L.; Sanborn, G.P.; Lacasse, P.A.; Gruenberg, K.M. & Ready, W.J. (2008) Improved Fracture Toughness of Carbon Fiber Composite Functionalized with Multi Walled Carbon Nanotubes. *Carbon,* Vol. 46, pp 2026-2033.

Fukuda, H. & Chou, T.W. (1982) A Probabilistic Theory of the Strength of Short-fiber Composites with Variable Fiber Length and Orientation. *Journal of Materials Science,* Vol. 17, pp 1003.

Kimura, T.; Ago, H.; Tobita, M.; Ohshima, S.; Kyotani, M. & Yumura, M. (2003) Polymer Composites of Carbon Nanotubes Aligned by a Magnetic Field. *Advanced Materials,* Vol. 14, No. 19, pp 1380-1383.

Krenchel, H. (1964) Fibre Reinforcement. Akademisk Forlag. Copenhagen.

Lau, K. (2003) Interfacial Bonding Characteristics of Nanotube/Polymer Composites. *Chemical Physics Letters,* Vol. 370, pp 399-405.

Lee, W.; Lee, S. & Kim C. (2006) The Mechanical Properties of MWNT/PMMA Nanocomposites Fabricated by Modified Injection Molding. *Composite Structures,* Vol. 76, pp 406-410.

Li, Y.; Hu, N.; Yamamoto, G.; Wang, Z.; Hashida, T.; Asanuma, H.; Dong, C.; Okabe, T.; Arai, M. & Fukunaga, H. (2010) Molecular Mechanics Simulation of the Sliding Behavior between Nested Walls in a Multi-walled Carbon Nanotube. *Carbon,* Vol. 48, pp 2934-2940.

Liao, K. & Li S. (2001) Interfacial Characteristics of a Carbon Nanotube-Polystyrene Composite System. *Applied Physics Letters,* Vol. 79, No. 25, pp 4225-4227.

Lordi, V. & Yao, N. (2000) Molecular Mechanics of Binding in Carbon-Nanotube-Polymer Composites. *Journal of Materials Research,* Vol. 15, No. 12, pp 2770-2779.

Marietta-Tondin, O. (2006) Molecular Modelling of Nanotube Composite Materials: Interface Formation, Interfacial Strength, and Thermal Expansion. The Florida State University. PhD Dissertation.

Natsuki, T.; Wang, F.; Ni, Q.Q. & Endo, M. (2007) Interfacial Stress Transfer of Fiber Pullout for Carbon Nanotubes with a Composite Coating. *Journal of Materials Science,* Vol. 42, pp 4191-4196.

Ogasawara, T.; Ishida, Y.; Ishikawa, T. & Yokota, R. (2004) Characterization of Multi-walled Carbon Nanotube/Phenylethynyl Termainated Polyimide Composites. *Composite: Part A,* Vol. 35, pp 67-74.

Qian, D.; Dickey, E.C.; Andrews, R. & Rantell, T. (2000) Load Transfer and Deformation Mechanisms in Carbon Nanotube-Polystyrene Composites. *Applied Physics Letters,* Vol. 76, No. 20, pp 2868-2870.

Rosca, I.D. & Hoa, S.V. (2009) Highly Conductive Multiwall Carbon Nanotube and Epoxy Composites Produced by Three-roll Milling. *Carbon,* Vol. 47, pp 1958-1968.

Safadi, B.; Andrews, R. & Grulke, E.A. (2002) Multiwalled Carbon Nanotube Polymer Composites: Synthesis and Characterization of Thin Films. *Journal of Applied Polymer Science,* Vol. 84, pp 2660-2669.

Schadler, L.S.; Giannaris, S.C. & Ajayan, P.M. (1998) Load Transfer in Carbon Nanotube Epoxy Composites. *Applied Physics Letters,* Vol. 73, No. 26, pp 3842-3844.

Sen, R.; Zhao, B.; Perea, D.; Itkis, M.E.; Hu, H.; Love, J.; Bekyarova, E. & Haddon, R.C. (2004) Preparation of Single-walled Carbon Nanotube Reinforced Polystyrene and Polyurethane Nanofibers and Membranes by Electrospinning. *Nano Letters,* Vol. 4, No. 3, pp 459-464.

Sun, H. (1998) COMPASS: An ab Initio Force-Field Optimized for Condensed-Phase Applications - Overview with Details on Alkane and Benzene Compounds. *Journal of Physical Chemistry B,* Vol. 102, No. 38, pp 7338-7364.

Tai, N.; Yeh, M. & Liu J. (2004) Enhancement of the Mechanical Properties of Carbon Nanotube/Phenolic Composites using a Carbon Nanotube Network as the Reiforcement. *Carbon,* Vol. 42, pp 2735-2777.

Thostenson, E.T.; Li, W.Z.; Wang, D.Z.; Ren, Z.F. & Chou, T.W. (2002) Carbon Nanotube/Carbon Fiber Hybrid Multiscale Composites. *Journal of Applied Physics,* Vol. 91, No. 9, pp 6034-6037.

Thostenson, E.T. & Chou TW. (2002) Aligned Multi-walled Carbon Nanotube-Reinforced Composites: Processing and Mechanical Characterization. *Journal of Physics D,* Vol. 35, pp L77-L80.

Tsai, J. & Lu, T. (2009) Investigating the Load Transfer Efficiency in Carbon Nanotubes Reinforced Nanocomposites. *Composite Structures,* Vol. 90, pp 172-179.

Veedu, V.P.; Cao, A.; Li, X.; Ma, K.; Soldano, C.; Kar, S.; Ajayan, P.M. & Ghasemi-Nejhad, M.N. (2006) Multifunctional Composites using Reinforced Laminae with Carbon-nanotube Forests. *Nature Materials,* Vol. 5, pp 457-462.

Vigolo, B.; Penicaud, A.; Coulon, C.; Sauder, C.; Pailler, R.; Journet, C.; Bernier, P. & Poulin, P. (2000) Macroscopic Fibers and Ribbons of Oriented Carbon Nanotubes. *Science,* Vol. 290, No. 17, pp 1331-1334.

Wong, M.; Paramsothy, M.; Xu, XJ.; Ren, Y.; Li, S. & Liao, K. (2003) Physical Interactions at Carbon Nanotube-Polymer Interface. *Polymer,* Vol. 44, pp 7757-7764.

Xiao, K.Q. & Zhang, L.C. (2004) The Stress Transfer Efficiency of a Single-walled Carbon Nanotube in Epoxy Matrix. *Journal of Materials Science,* Vol. 39, pp 4481-4486.

Yokozeki, T.; Iwahori, Y. & Ishiwata, S. (2007) Matrix Cracking Behaviors in Carbon Fiber/Epoxy Laminates Filled with Cup-stacked Carbon Nanotubes (CSCNTs). *Composites Part A,* Vol. 38, pp 917-924.

Zheng, Q.; Xia, D.; Xue, Q.; Yan, K.; Gao, X. & Li Q. (2009) Computational Analysis of Effect of Modification on the Interfacial Characteristics of a Carbon Nanotube-Polyethylene Composites System. *Applied Surface Science,* Vol. 255, pp 3524-3543.

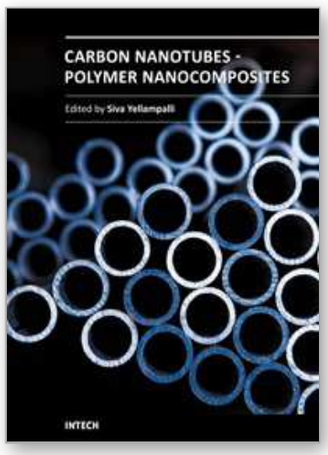

Carbon Nanotubes - Polymer Nanocomposites

Edited by Dr. Siva Yellampalli

ISBN 978-953-307-498-6
Hard cover, 396 pages
Publisher InTech
Published online 17, August, 2011
Published in print edition August, 2011

Polymer nanocomposites are a class of material with a great deal of promise for potential applications in various industries ranging from construction to aerospace. The main difference between polymeric nanocomposites and conventional composites is the filler that is being used for reinforcement. In the nanocomposites the reinforcement is on the order of nanometer that leads to a very different final macroscopic property. Due to this unique feature polymeric nanocomposites have been studied exclusively in the last decade using various nanofillers such as minerals, sheets or fibers. This books focuses on the preparation and property analysis of polymer nanocomposites with CNTs (fibers) as nano fillers. The book has been divided into three sections. The first section deals with fabrication and property analysis of new carbon nanotube structures. The second section deals with preparation and characterization of polymer composites with CNTs followed by the various applications of polymers with CNTs in the third section.

INTECH
open science | open minds

InTech Europe
University Campus STeP Ri
Slavka Krautzeka 83/A
51000 Rijeka, Croatia
Phone: +385 (51) 770 447
Fax: +385 (51) 686 166
www.intechopen.com

InTech China
Unit 405, Office Block, Hotel Equatorial Shanghai
No.65, Yan An Road (West), Shanghai, 200040, China
中国上海市延安西路65号上海国际贵都大饭店办公楼405单元
Phone: +86-21-62489820
Fax: +86-21-62489821

IntechOpen